Quantities of Interest for Surface based Resistivity Geophysical Measurements

J. Alvarez-Aramberri[1,2,3], S.A. Bakr[1,4], D. Pardo[2,5,1], and H. Barucq[6]

[1] BCAM - Basque Center for Applied Mathematics, Bilbao, Basque Country, Spain.
{julen.alvarez.aramberri,shaaban.bakr1,dzuabiaur}@gmail.com
[2] University of the Basque Country (UPV/EHU), Bilbao, Basque Country, Spain.
[3] University of Pau (UPPA), Pau, France.
[4] Department of Mathematics, Assiut University, Assiut, Egypt
[5] IKERBASQUE, Basque Foundation for Science, Bilbao, Basque Country, Spain.
[6] EPC Magique-3D, Inria, LMA, University of Pau, F64013 Pau, France.
helene.barucq@inria.fr

Abstract
The objective of traditional goal-oriented strategies is to construct an *optimal* mesh that minimizes the problem size needed to achieve a user prescribed tolerance error for a given quantity of interest (QoI). Typical geophysical resistivity measurement acquisition systems can easily record electromagnetic (EM) fields. However, depending upon the application, EM fields are sometimes loosely related to the quantity that is to be inverted (conductivity or resistivity), and therefore they become inadequate for inversion. In the present work, we study the impact of the selection of the QoI in our inverse problem. We focus on two different acquisition systems: marine controlled source electromagnetic (CSEM), and magnetotellurics (MT). For both applications, numerical results illustrate the benefits of employing adequate QoI. Specifically, the use as QoI of the impedance matrix on MT measurements provides significant computational savings, since one can replace the existing absorbing boundary conditions (BCs) by a homogeneous Dirichlet BC to truncate the computational domain, something that is not possible when considering EM fields as QoI.

Keywords: Quantities of Interest, Finite Element Method, Secondary Field Formulation, Magnetotelluric Problem, Marine CSEM, Goal-Oriented Adaptivity, Inverse Problems.

1 Introduction

A map of the Earth's subsurface is employed in multiple applications, including hydrocarbon exploration, CO_2-sequestration, and oil prospection. To obtain such a map, multiple measurements can be recorded (such as EM, elasto-acoustics, and nuclear) both on the surface or using logging instruments. These measurements are subsequently inverted to obtain the material properties of the Earth's subsurface, and hence, to *image* it.

In the present work, we consider two different on surface resistivity acquisition systems: marine controlled source electromagnetics (CSEM) [7] and magnetotellurics (MT) [15], both governed by Maxwell's equations. These two scenarios are depicted in Figure 1. In marine

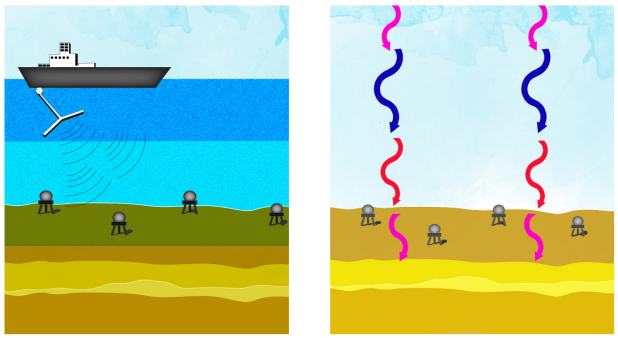

Marine CSEM Magnetotelluric Problem

Figure 1: Two different resistivity measurement acquisition systems for the characterization of the Earth's subsurface.

CSEM, a towed electric-dipole repeatedly generates electric fields at different locations, and the response after interacting with the geological formation is recorded by the seafloor receivers. Depending on the depth of the target area, the transmitter operating frequencies may range from 0.1 to 10 Hz and the source-receiver offsets can be up to 10 km (see, e.g., [7]). In MT, natural sources located at the ionosphere are responsible for the MT signals. The receivers in MT are equivalent to CSEM receivers; hence, it is possible to record both MT and CSEM measurements in one survey and employ them together for an improved understanding of the subsurface geology.

While the above measurement acquisition systems can easily record EM fields, these may be of no interest for inversion. In particular, for MT, the intensity of the source is unknown, and therefore it is impossible to invert for the electric and magnetic fields, which directly depend on it. As a result, the inversion is often performed with data based on impedances (or a postprocessed quantity from the impedance, e.g. the apparent resistivity [16]).

In marine CSEM, the recorded EM fields contain information both about the subsurface and the wave traveling throughout the sea, and possibly the air in shallow waters. The wave traveling through the water and air contains no valuable information for inversion. Thus, it is convenient to remove it from our measurements. This can be achieved by considering a secondary field formulation [3].

The QoI for the adaptive process should ideally match with that employed for the inversion. In the present work, we study various QoI that are suitable for inversion in MT and marine CSEM. A proper selection of a QoI is essential to obtain optimal results when employing goal-oriented adaptivity [13, 14].

The main contribution of this paper is to illustrate how some QoI are more related to the material properties than others. Moreover, we show that discretization errors associated to the EM fields and to the QoI used for inversion highly differ, especially when the full formulation is employed. One extreme example of this situation corresponds to the case of MT, where a perfectly matched layer (PML) [2] is unnecessary when computing impedances rather than EM fields. This provides further computational savings.

We solve the forward MT problem with an *hp*-Finite Element Method (FEM) [6, 8], employing a multigoal-oriented strategy (proposed in [10]) to build the *hp*-grid. The simulations

of 3D marine CSEM measurements are obtained with a domain decomposition method [4].

The present paper is organized as follows: we start with the formulation of the problem in Section 2. Then, in Section 3 we describe which QoI are interesting for the considered geophysical electromagnetic applications. Section 4 is devoted for numerical results and finally, in Section 5 we provide some conclusions and point out to some future research directions.

2 Formulation

Assuming a time-harmonic dependence of the form $e^{j\omega t}$, pre-multiplying both sides of Faraday's law by $\boldsymbol{\mu}^{-1}$, applying the curl, and using Ampère's law, we obtain the *reduced wave equation*,

$$\boldsymbol{\nabla} \times (\boldsymbol{\mu}^{-1} \boldsymbol{\nabla} \times \boldsymbol{E}) - \boldsymbol{k}^2 \boldsymbol{E} = -j\omega \boldsymbol{J}^{imp} - \boldsymbol{\nabla} \times (\boldsymbol{\mu}^{-1} \boldsymbol{M}^{imp}), \tag{1}$$

where $\boldsymbol{k}^2 = \omega^2 \boldsymbol{\varepsilon} - j\omega \boldsymbol{\sigma}$. Here, $\boldsymbol{E}$ corresponds to the electric field, driven by an impressed prescribed electric and magnetic density current sources, $\boldsymbol{J}^{imp}$ and $\boldsymbol{M}^{imp}$. j is the imaginary unit, ω is the angular frequency, $\boldsymbol{\sigma}$ stands for the conductivity of the media, $\boldsymbol{\varepsilon}$ for the electrical permitivity, and $\boldsymbol{\mu}$ for the magnetic permeability. We assume that the material properties are given by diagonal 3×3 matrices with σ, ε_0 and μ_0 in their diagonals, respectively, where ε_0 and μ_0 are assumed to be these of vacuum.

Secondary Field Formulation: A possible approach for solving Maxwell's equations consists of splitting the electric and magnetic fields into their primary and secondary components. The first one corresponds to the fields arisen from some reference conductivity model $\boldsymbol{\sigma}^P$ while the second one arises from the difference between the actual conductivity distribution $\boldsymbol{\sigma}$, with respect to the reference model, that is, $\boldsymbol{\sigma}^S = \boldsymbol{\sigma} - \boldsymbol{\sigma}^P$. Then, being Ω_S the domain where the higher dimensional inhomogeneities are located, $\boldsymbol{\sigma}^S$ is equal to zero outside Ω_S.

Thus, the equation for the secondary electric field (1) becomes:

$$\boldsymbol{\nabla} \times \left(\boldsymbol{\mu}^{-1} \boldsymbol{\nabla} \times \boldsymbol{E}^S \right) - \boldsymbol{k}^2 \boldsymbol{E}^S = -j\omega \boldsymbol{\sigma}^S \boldsymbol{E}^P, \tag{2}$$

where $\boldsymbol{E}^P$ corresponds to the primary field and $\boldsymbol{E}^S$ is the secondary field, which equals to $\boldsymbol{E}^S = \boldsymbol{E} - \boldsymbol{E}^P$.

2.1 Variational Formulation

We define the L^2-inner product of two possibly complex and vector valued functions $\boldsymbol{f_1}$ and $\boldsymbol{f_2}$ as:

$$\langle \boldsymbol{f_1}, \boldsymbol{f_2} \rangle_{L^2(\Omega)} = \int_\Omega \boldsymbol{f_1}^* \boldsymbol{f_2} \, d\Omega, \tag{3}$$

where $\boldsymbol{f}^*$ denotes the adjoint (transpose of the complex conjugate) of $\boldsymbol{f}$. We pre-multiply both sides of equation (2) by the adjoint $\boldsymbol{F}^*$ of a vector-valued test function $\boldsymbol{F} \in V(\Omega) = \{\boldsymbol{F} \in \boldsymbol{L}^2(\Omega) : (\boldsymbol{n} \times \boldsymbol{F})|_{\Gamma_D} = 0, \ \boldsymbol{\nabla} \times \boldsymbol{F} \in \boldsymbol{L}^2(\Omega)\}$, integrate by parts over domain Ω, and incorporate the perfect electrically conductive boundary condition $(\boldsymbol{n} \times \boldsymbol{E})|_{\Gamma_D} = 0$. Thus, the variational formulation for the secondary field is given by:

$$\begin{cases} \text{Find} \quad \boldsymbol{E}^S \in V(\Omega), \quad \text{such that:} \\ \langle \boldsymbol{\nabla} \times \boldsymbol{F}, \boldsymbol{\mu}^{-1} \boldsymbol{\nabla} \times \boldsymbol{E}^S \rangle_{L^2(\Omega)} - \langle \boldsymbol{F}, \boldsymbol{k}^2 \boldsymbol{E}^S \rangle_{L^2(\Omega)} = -j\omega \langle \boldsymbol{F}, \boldsymbol{\sigma}^S \boldsymbol{E}^P \rangle_{L^2(\Omega)}, \quad \forall \boldsymbol{F} \in V(\Omega), \end{cases} \tag{4}$$

2D Case: Transverse Electric (TE) Mode. Our aim is to find the y component of the electric field $E_y(x,z) \in \Omega$, satisfying the homogeneous Dirichlet BCs and equation (1). The corresponding variational formulation is analogously obtained, where now $V(\Omega) = \{F \in L^2(\Omega) : F|_{\Gamma_D} = 0, \boldsymbol{\nabla} F \in \boldsymbol{L}^2(\Omega)\}$ and $\partial/\partial y = 0$.

2.2 Solution Method

We employ an *hp*-FEM [6] to solve the forward MT problem. Since we have more than one receiver, we need to simultaneously compute several quantities of interest (one per receiver). Therefore, for the 2D computations, we employ a multigoal-oriented strategy, proposed in [10] and employed also in [1], where a new linear QoI that takes into account all receivers is used. The simulations of 3D marine CSEM measurements are obtained with a domain decomposition method [4]. It combines H(**curl**) finite elements with Fourier basis functions. The zones of the computational domain where it is reasonable to represent geoelectric properties in 2D are discretized by combining 2D FE with a Fourier series [12]. The remaining part is discretized utilizing traditional H(**curl**) 3D FE methods. The resulting discretization delivers highly accurate simulations of marine CSEM problems with arbitrary 3D geometries while it considerably reduces the computational complexity of full 3D FE simulations for typical marine CSEM problems.

3 Quantities of Interest

In the scope of subsurface modelling, the choice of the QoI is important for both, direct and inverse problems. In marine CSEM, the EM fields are typically employed for inversion. In MT, due to the lack of knowledge of the source properties, the impedance tensor or a postprocessed quantity from the impedance is employed.

The traditional theory of goal-oriented adaptivity employs as QoI a linear and continuous functional [11] in u associated to the i-th receiver and defined as

$$L^i(u) = \frac{1}{|\Omega_{R^i}|} \int_{\Omega_{R^i}} u \, d\Omega, \tag{5}$$

where Ω_{R^i} is the domain occupied by the i-th receiver and u corresponds to some component of the electric or magnetic field. Thus, for the secondary field formulation, because of the linearity of L^i (omitting the i-th super script for the sake of simplicity from now on), we have that for each receiver

$$L(u) = L(u^P) + L(u^S). \tag{6}$$

To only employ a linear QoI is a significant restriction. Therefore, in addition to linear QoI, we also study the performance of nonlinear ones. In MT, our aim is to obtain retry information of the electric conductivity distribution of the subsurface. Since the MT source intensity is unknown, it is then necessary to define a QoI independent of it. A good candidate for this purpose is the impedance matrix $\mathcal{Z}$, a nonlinear quantity that is given by the ratio between the electric and magnetic fields. For the 2D MT problem, two uncoupled modes can be derived from Maxwell's equations, the so called transverse electric (TE) and transverse magnetic (TM) modes. Then, we define impedances related to each of them as:

$$\mathcal{Z}_{TE} = \mathcal{Z}_{yx} = \frac{E_y}{H_x}, \qquad \mathcal{Z}_{TM} = \mathcal{Z}_{xy} = \frac{E_x}{H_y}. \tag{7}$$

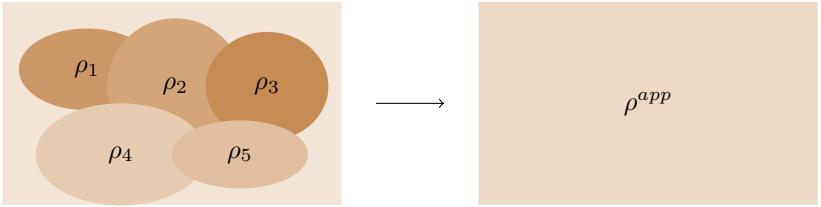

Figure 2: Illustration of the apparent resistivity.

Here, we compute E_y and H_y with a 2D *hp*-FEM [6] and H_x and E_x are obtained from Maxwell's equations according to the postprocessing formulas:

$$H_x = \frac{1}{j\omega\mu}\frac{\partial E_y}{\partial z}, \qquad E_x = -\frac{1}{\sigma + j\omega\varepsilon}\frac{\partial H_y}{\partial z}. \tag{8}$$

To see the relation between the impedance matrix and the subsurface resistivity distribution, we consider a simple one-dimensional case given by a stratified model over which a linearly polarized plane wave incides. For this case, Cagniard [5] showed in 1953 that the solution in each layer n of height h_n is given by:

$$E_y^n(z,\omega) = A_n e^{j\gamma_n z} + B_n e^{-j\gamma_n z}, \qquad H_x^n(z,\omega) = \frac{\gamma_n}{\omega\mu}(A_n e^{j\gamma_n z} - B_n e^{-j\gamma_n z}), \tag{9}$$

where coefficients A_n and B_n are dependent of interface conditions. $\gamma_n = \sqrt{j\omega\mu\sigma_n - \omega^2\mu\varepsilon}$ and σ_n are the wavenumber and conductivity associated to the n-th layer. The impedance at the surface is then given by:

$$\mathcal{Z}_{kl} = \frac{E_k^1(z=0)}{H_l^1(z=0)} = \frac{A_1 + B_1}{A_1 - B_1}\frac{\omega\mu}{\gamma_1} = C(n, \sigma_1, \ldots, \sigma_n, h_1, \ldots, h_n, \omega)\frac{\omega\mu}{\gamma_1}, \tag{10}$$

where k and l can be either x or y. The impedance is then independent of the source $\boldsymbol{J}^{imp}$. In particular, for the half-space case, $C = \pm 1$ (depending upon the involved fields) in the above definition and therefore,

$$\mathcal{Z}_{kl} = \frac{\omega\mu}{\gamma_1} = \frac{\omega\mu}{\sqrt{j\omega\mu\sigma - \omega^2\mu\varepsilon}} \simeq \pm\frac{\omega\mu}{\sqrt{j\omega\mu\sigma}}. \tag{11}$$

Then, it is possible to define the *apparent resistivity* of the media as

$$\rho_{kl}^{app} = \frac{1}{\sigma_{kl}^{app}} = \frac{1}{\omega\mu}|\mathcal{Z}_{kl}|^2. \tag{12}$$

which in the special case of the half-space corresponds to the actual one. For more complex scenarios it is then an approximation which corresponds to an average of the subsurface resistivities, as illustrated in Figure 2. Thus, it is directly related with the actual subsurface resistivity distribution.

We focus on the electric field and compute it in two different ways. First, we employ the full field formulation, and compute the total electric field at the receivers, which we denote

as $Q_E^F(\sigma)$. Second, we use the secondary field formulation, consider the secondary field as the QoI, and compute it numerically. After that, we calculate the total field at the receivers by incorporating the primary field solution obtained analytically (or semi-analytically in the case of marine CSEM). We denote it by $Q_E^S(\sigma)$. The same approach is followed for the impedance, and the resulting quantities are denoted as $Q_Z^F(\sigma)$ and $Q_Z^S(\sigma)$, respectively.

Thus, $Q_E^F(\sigma)$ and $Q_Z^F(\sigma)$ correspond to the quantities obtained with the full field formulation, while $Q_E^S(\sigma)$ and $Q_Z^S(\sigma)$ to the ones computed with the secondary field formulation. In the next section, we compare the performance of these quantities.

4 Numerical Results

In this section, we study how the selection of the QoI affects to the accuracy of our forward direct solver.

4.1 MT

The physical problem is illustrated in Figure 3a. The computational domain consists of air (above) and a layered media containing some 2D inhomogeneities. To treat the incoming electromagnetic fields as plane waves that propagate in the vertical direction towards the Earth's surface, we model the source (located at the ionosphere and represented with a dark blue rectangle) as an infinitely long (in x and y directions) rectangular surface. The receivers (red crosses) are located at the Earth's surface. Figure 3a illustrates the computational domain when the secondary field formulation is considered. The light area represents the new (smaller) computational domain. In this case, the source is located at the 2D inhomogeneities, namely, the box with conductivity ρ_4. In both cases, the physical domain is truncated with a PML. The relative permittivity and permeability are the same for all materials, and equal to one. The values for the conductivity are $(\rho_1, \rho_2, \rho_3, \rho_4) = (3, 2, 4, 200)$ Ohm.m, the frequency 0.05 Hz, and the forcing term $J_y^{imp} = 1$.

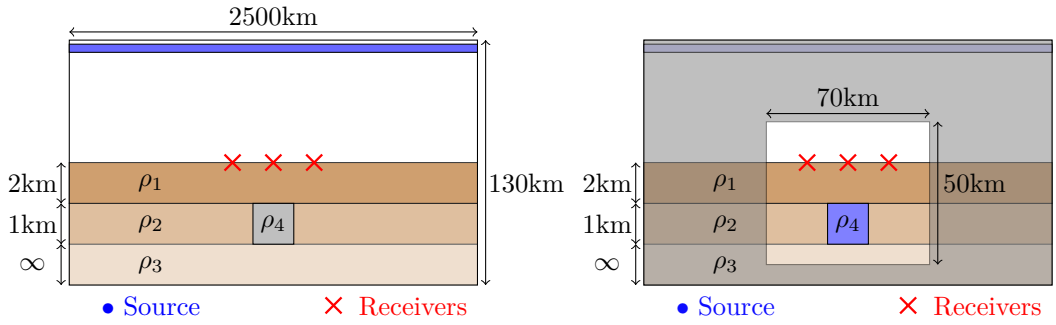

(a) Full field formulation

(b) Secondary field formulation

Figure 3: Computational domain for the 2D MT problem.

In the following figures, we represent the relative error between the numerical and reference solutions against the number of unknowns. In all of them, the increase in the unknowns comes from global refinements in h and/or p, while the reference solution always corresponds to an overkill solution, computed with the multigoal-oriented algorithm [10]. This algorithm needs linear QoI to perform the adaptivity, and since the impedance is nonlinear, we employ the

electric field. In the particular case of the impedance, which up to a constant, it corresponds to the electric field divided by its derivative, we can ensure the goodness of the reference solutions. The relative error is defined between these two solutions at the center of the domain, which is the region more influenced by the presence of the inhomogeneity.

In a first step, we compare the electric field and impedance as QoI for both, full and secondary field formulations. In Figures 4a and 4c (left column) we display the relative error for the electric field and the impedance with the full field formulation, while in Figures 4b and 4d (right column) we employ the secondary field formulation. In both cases, the impedance provides more accurate results than the electric field itself, especially for the full field formulation, where the difference is by several orders of magnitude. For the secondary field formulation, the advantage of using the impedance as QoI diminishes, although it still exhibits a smaller error. If we compare the errors given by both formulations, for the electric field ($Q_E^F(\sigma)$ and $Q_E^S(\sigma)$) and for the impedance ($Q_Z^F(\sigma)$ and $Q_Z^S(\sigma)$), it is clear that the secondary field formulation always provides smaller errors for both physical magnitudes, even more for the electric field, which shows a large error (up to a 30%), when a coarse mesh is employed.

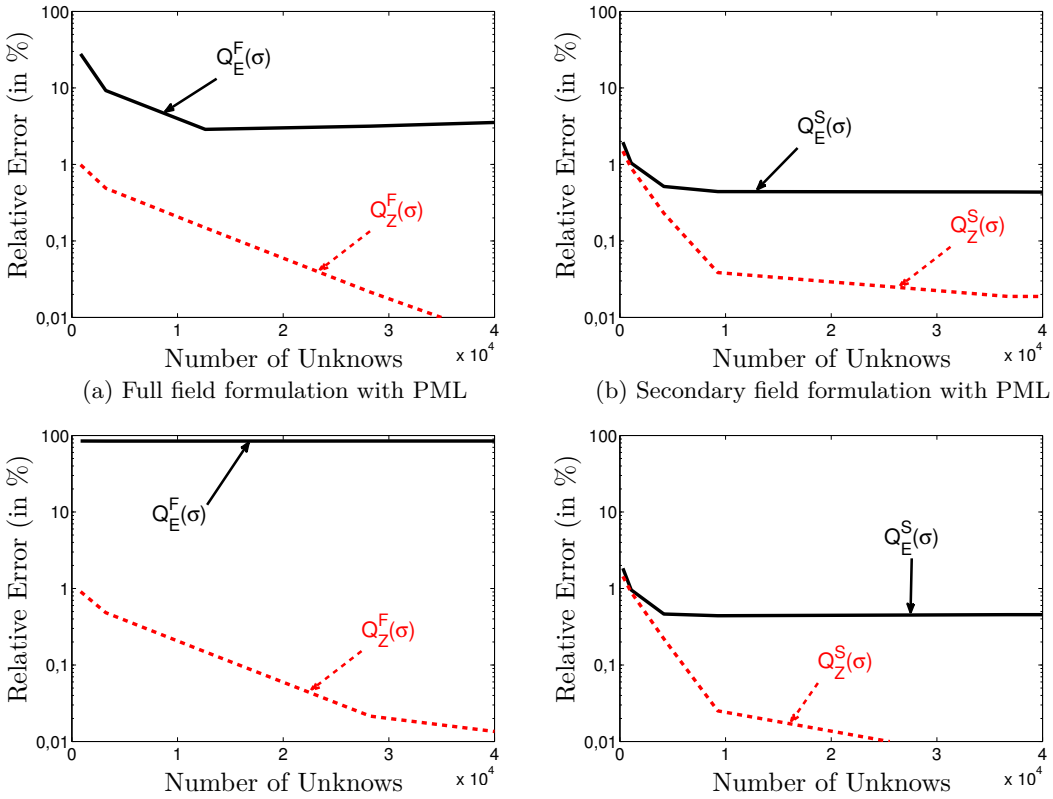

(a) Full field formulation with PML

(b) Secondary field formulation with PML

(c) Full field formulation without PML

(d) Secondary field formulation without PML

Figure 4: Relative error for different QoI without PML. $Q_E^F(\sigma)$ and $Q_Z^F(\sigma)$ correspond to the total electric field and the impedance computed with the full formulation, respectively, while $Q_E^S(\sigma)$ and $Q_Z^S(\sigma)$ to the ones computed with the secondary field formulation.

First, we employ the full field formulation, and compute the total electric field at the re-

ceivers, which we denote as $Q_E^F(\sigma)$. Second, we use the secondary field formulation, consider the secondary field as the QoI, and compute it numerically. After that, we calculate the total field at the receivers incorporating the primary field solution obtained analytically (or semi-analytically in the case of marine CSEM). We denote it by $Q_E^S(\sigma)$. The same approach is followed for the impedance and the resulting quantities are denoted as $Q_Z^F(\sigma)$ and $Q_Z^S(\sigma)$, respectively.

We now compute the same QoI without considering a PML. Being the air a non dissipative media, and since we employ Dirichlet homogeneous boundary conditions for truncation purposes, we expect to have numerical reflections from the boundary and hence inaccurate results. We again compare in Figures 4c and 4d the electric field and the impedance when employing the full and the secondary field formulation, respectively. In the first case, the electric field solution contains 100% relative error even when the number of unknowns in large, as expected. However, the impedance shows a superb accuracy. Now it is unnecessary any effort in the truncation of the domain, which in general procure savings in both, computational complexity and implementation tasks. When the secondary field is employed, we obtain acceptable results for the electric field due of the attenuation of the source, which is embedded in a lossy media. However, we still observe that the relative error does not converge to zero when computing the electric field, while the impedance rapidly convergences.

We conclude that the impedance is not only more closely related to the formation conductivity, but it also provides dramatically smaller discretization errors, leading to large computational savings. As a result, the impedance is a better choice as QoI in comparison with the electric field.

4.2 Marine CSEM

In this subsection, we compare the relative error for FFE method when applied to solve the full vs secondary field formulations. The frequency excited by the horizontal electric dipole is equal to 0.25 Hz and the transmitter is located 50 m above the sea-floor with (x, y) coordinates equal to $(0, 0)$. There are ten equally spaced receivers located on the sea-floor at horizontal distances varying from 1 km to 10 km.

The horizontally stratified geoelectric model (1D model) considered here to compute the primary field ($\mathbf{E}^P$) consists of an air layer with resistivity 10^8 Ohm.m, a seawater layer with thickness 1.5 km and resistivity 0.3 Ohm.m, a sea-bottom layer with thickness 1.1 km and resistivity 1.0 Ohm.m, a layer with thickness 1.1 km and resistivity 2 Ohm.m, a layer with thickness 500 m and resistivity 1.5 Ohm.m, and a more resistive basement layer with resistivity 5 Ohm.m.

The 3D model is derived from the 1D geoelectric one by including a 3D resistive target (resistivity equals to 100 Ohm.m) with finite size in all axes directions. The geoelectric model is illustrated in Fig. 5. The extension of the resistive target (black color) is 3 km, 6 km and 100 m in the x, y and z directions, respectively.

Figure 6a describes the relative error (integral equation (IE) method (see, e.g., [9]) versus FFE method) in percent of the electric field obtained with FFE method for the full field formulation (solid line) and the secondary field formulation (dashed line) when applied to the model problem of Figure 5. The FFE method for the secondary field formulation delivers very accurate results with a significantly lower number of unknowns. About 25% of the unknowns is sufficient to provide a better accuracy when using the secondary field formulation. An error level below 10% is acceptable and corresponds to what it is considered an accurate solution in the context of marine CSEM measurements, since the anomaly produced by the presence of an oil box is considerably larger (between 10% and 80%, See Figure 6b). Figure 6b shows the

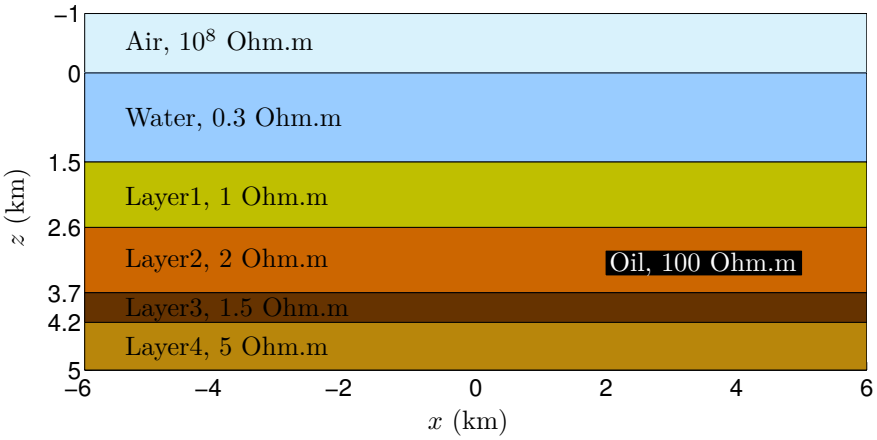

Figure 5: Central portion of the vertical cross section of the geoelectric model with 3D target.

sensitivity of both formulations to the subsurface resistivity distribution. The secondary field formulation is more sensitive to the materials properties than the full field formulation.

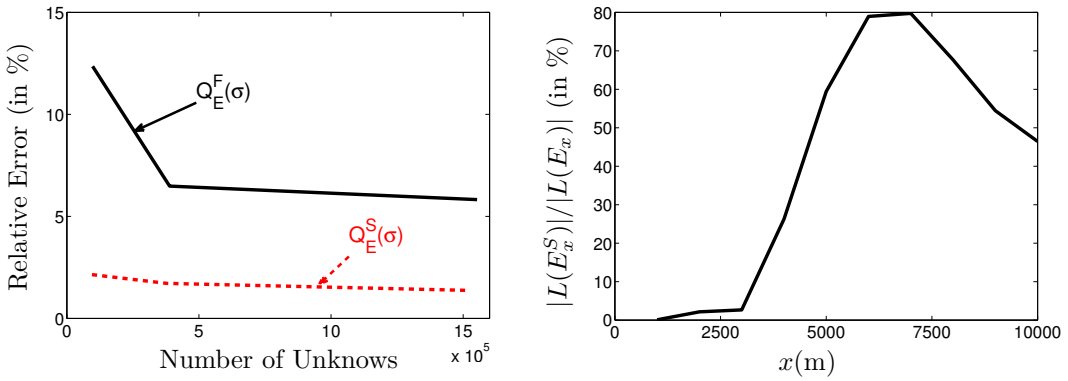

(a) Relative error (IE versus FFE)

(b) Anomaly's relative size produced by the oil box

Figure 6: Numerical results for marine CSEM.

5 Conclusions

We have analyzed the selection of the QoI in the context of two resistivity geophysical applications: MT and marine CSEM. In both cases, we observe that the secondary field formulation provides higher accuracy, and it is more sensitive to variations in the subsurface conductivity distribution. Therefore, one should refrain from using the total EM field as QoI. Additionally, for the particular case of MT, we show that discretization errors of EM fields and the impedance matrix highly differ. In particular, computing impedances rather than EM fields provides high computational savings. Additionally, the use of impedances enable to accurately solve the problem even when employing simply homogeneous Dirichlet BCs to truncate the computational

domain.

Acknowledgments This research is supported by the Project of the Spanish Ministry of Economy and Competitiveness with reference MTM2013-40824-P, the BCAM "Severo Ochoa" accreditation of excellence SEV-2013-0323, the CYTED 2011 project 712RT0449, and the Basque Government through the BERC 2014-2017 program and the Consolidated Research Group Grant IT649-13 on "Mathematical Modeling, Simulation, and Industrial Applications (M2SI)", and the RISE Horizon 2020 European Project GEAGAM (644602).

References

[1] J. Alvarez-Aramberri, D. Pardo, and H. Barucq. Inversion of magnetotelluric measurements using multigoal oriented *hp*-adaptivity. *Proc. Comput. Sci.*, 18:1564–1573, 2013.

[2] J. Alvarez-Aramberri, D. Pardo, and H. Barucq. A secondary field based *hp*-finite element method for the simulation of magnetotelluric measurements. *J. Comput. Sci.*, Accepted.

[3] S.A. Bakr and D. Pardo. A secondary field based fourier finite element method for the simulation of 3d marine csem measurements. *2014 SEG Annual Meeting, 26-31 October, Denver, Colorado, USA*, page 1089, 2014.

[4] S.A. Bakr, D. Pardo, and T. Mannseth. Domain decompostion fourier finite element method for the simulation of 3d marine csem measurements. *J. Comput. Phys.*, 255:456–470, 2013.

[5] L. Cagniard. Basic theory of the magnetotelluric method of geophysical prospecting. *Geophysics*, 18(3):605–635, 1953.

[6] L. Demkowicz. *Computing with hp-Adaptive Finite Elements: Volume 1 One and Two Dimensional Elliptic and Maxwell problems*. CRC Press, 2006.

[7] T. Eidesmo, S. Ellingsrud, L.M. MacGregor, S. Constable, M.C. Sinha, S.E. Johansen, F.N. Kong, and H. Westerdahl. Sea bed logging (sbl), a new method for remote and direct identification of hydrocarbon filled layers in deepwater areas. *First break*, 20(3), 2002.

[8] I. Gomez-Revuelto, L.E. Garcia-Castillo, S. Llorente-Romano, and D. Pardo. 3d *hp*-adaptive finite element simulations of bend, step, and magic-T electromagnetic waveguide structures. *J. Comput. Sci.*, 5(2):65 – 75, 2014.

[9] G. Hursán and M. Zhdanov. Contraction integral method in three-dimensional electromagnetic modeling. *Radio Science*, 37:1089, 2002.

[10] D. Pardo. Multigoal-oriented adaptivity for *hp*-finite element methods. *Proc. Comput. Sci.*, 1(1):1953–1961, 2010.

[11] D. Pardo, L. Demkowicz, C. Torres-Verdin, and M. Paszynski. A self-adaptive goal-oriented *hp*-finite element method with electromagnetic applications. part ii: Electrodynamics. *Comput. Methods Appl. Mech. Eng.*, 196(37):3585–3597, 2007.

[12] D. Pardo, M.J. Nam, C. Torres-Verdin, M.G. Hoversten, and I. Garay. Simulation of marine controlled source electromagnetic measurements using a parallel fourier *hp*-finite element method. *Comput. Geosci.*, 15:53–67, 2011.

[13] S. Prudhomme and J. T. Oden. On goal-oriented error estimation for elliptic problems: application to the control of pointwise errors. *Comput. Methods Appl. Mech. Eng.*, 176(1):313–331, 1999.

[14] R. Rannacher and F.T. Suttmeier. A posteriori error control in finite element methods via duality techniques: Application to perfect plasticity. *Computational mechanics*, 21(2):123–133, 1998.

[15] F. Simpson and K. Bahr. *Practical magnetotellurics*. Cambridge University Press, 2005.

[16] B.R. Spies and D.E. Eggers. The use and misuse of apparent resistivity in electromagnetic methods. *Geophysics*, 51(7):1462–1471, 1986.